Ionics (2016) 22:593–600
DOI 10.1007/s11581-015-1572-2

ORIGINAL PAPER

Fabrication of bimetallic Pt/Pd nanoparticles on 2-thiolbenzimidazole functionalized reduced graphene oxide for methanol oxidation

Onur Akyıldırım[1] · Gül Kotan[2] · Mehmet Lütfi Yola[3] · Tanju Eren[4] · Necip Atar[4]

Received: 10 September 2015 / Revised: 21 September 2015 / Accepted: 27 September 2015 / Published online: 8 October 2015

Abstract In this study, an electrocatalyst based on 2-thiolbenzimidazole (TBI) functionalized reduced graphene oxide (rGO) with platinum and palladium nanoparticles (Pt-PdNPs) was synthesized. The successful synthesis of nanomaterials and the prepared glassy carbon electrode (GCE) surfaces were confirmed by transmission electron microscope, X-ray photo electron spectroscopy, scanning electron microscope, electrochemical impedance spectroscopy and X-ray diffraction method. The effective surface areas of TBIrGO/GCE, PdNPs/TBIrGO/GCE, PtNPs/TBIrGO/GCE and Pt-PdNPs/TBIrGO/GCE were calculated to be 324, 578, 667 and 1189 cm^2/mg, respectively. According to the results, the electrochemical surface area of the Pt-PdNPs/TBIrGO is 3.67, 2.06 and 1.78 times higher than those of TBIrGO, PdNPs/TBIrGO and PtNPs/TBIrGO, respectively. The Pt-PdNPs/TBIrGO/GCE also exhibited higher peak current for methanol oxidation than those of comparable TBIrGO/GCE, PdNPs/TBIrGO/GCE, PtNPs/TBIrGO/GCE modified GCEs, thus providing evidence for its higher electro-catalytic activity.

✉ Onur Akyıldırım
onurakyildirim@gmail.com

✉ Necip Atar
necipatar@gmail.com; natar@pau.edu.tr

[1] Department of Chemical Engineering, Faculty of Engineering and Architecture, Kafkas University, Kars, Turkey

[2] Department of Chemistry, Faculty of Science and Letters, Kafkas University, Kars, Turkey

[3] Department of Metallurgical and Materials Engineering, Faculty of Engineering, Sinop University, Sinop, Turkey

[4] Department of Chemical Engineering, Faculty of Engineering, Pamukkale University, Denizli, Turkey

Keywords Reduced graphene oxide · 2-Thiolbenzimidazole · Nanoparticle · Methanol oxidation

Introduction

Fuel cells can generate energy from various fuels and they have been important method in terms of electricity production. Especially, direct-methanol fuel cells (DMFCs) are proton-exchange fuel cell in which methanol is used as the fuel. Their important advantages are the simplicity of transport of methanol. Methanol as fuel has several advantages such as transport and storage. DMFCs have been used for the production of energy for the several years. A sulfuric acid or perchloric acid as supporting electrolyte is used in the DMFCs owing to removing of the CO_2 during the electrochemical progress [1–3]. The reaction of methanol oxidation in an acidic medium can be presented as below [3, 4].

$$(\text{Anode})CH_3OH + H_2O \rightarrow CO_2 + 6H^+ + 6e^- \qquad E^\circ = 0.043V(\text{SHE})$$
$$(\text{Cathode})3/2O_2 + 6H^+ + 6e^- \rightarrow 3H_2O \qquad E^\circ = 1.229V(\text{SHE})$$

(The all electrochemical reaction):

$$CH_3OH + 3/2O_2 \rightarrow CO_2 + 2H_2O \qquad E^\circ = 1.186V(\text{SHE})$$

Especially, various nanomaterials and nanoparticles can been used for the development of energy, sensor and catalytic effect [5–14]. In addition, significant progress has been performed in the production of carbon-supported catalysts for fuel cells with suitable cost [15]. Nevertheless, there are some important problems such as low catalytic performance for methanol and ethanol oxidation. Hence, in order to increase this performance, the novel nanomaterials such as graphene/graphene oxide and carbon nanotubes become very significant [16–18]. In addition, some nanoparticles such as mono/

bimetallic are important in nano/sensor technology [19]. In addition, because the nano-sized particles have larger specific surface area, they are good catalysts [20]. The bimetallic nanoparticles can increase the rate of electrochemical reaction [21–23].

In the present report, the preparation and characterization of nanocomposites such as reduced graphene oxide (rGO), 2-thiolbenzimidazole (TBI)rGO/glassy carbon electrode (GCE), palladium nanoparticles (PdNPs)/TBIrGO, platinum nanoparticles (PtNPs)/TBIrGO and platinum and palladium nanoparticles (Pt-PdNPs)/TBIrGO were firstly performed (Scheme 1). After that, GCE surfaces were modified with these nanomaterials by using infrared heat lamp. The developed surfaces were characterized by electrochemical impedance spectroscopy (EIS), cyclic voltammetry (CV) and chronoamperometry (CA) measurements. After the characterizations of the glassy carbon surfaces, these catalysts were investigated for their effects in fuel cell applications.

Experimental

Materials

All chemicals that were used in the experiments were reagent grade and were used as received including the following: graphite powder (Merck, Germany), 2-thiolbenzimidazole (Merck, Germany), sodium tetrachloropalladate (Na_2PdCl_4, Merck, Germany), sulfuric acid (H_2SO_4, Merck, Germany), potassium persulfate ($K_2S_2O_8$, Merck, Germany), phosphorus pentoxide (P_2O_5, Merck, Germany), potassium permanganate ($KMnO_4$, Merck, Germany), hydrogen peroxide (H_2O_2, Merck, Germany), ethanol (Merck, Germany), hydrochloric acid (HCl, Sigma-Aldrich), N-(3-dimethylaminopropyl)-N-ethylcarbodiimidehydrochloride (EDC, Sigma-Aldrich, USA), ethanol (Sigma-Aldrich, USA), isopropyl alcohol (IPA, Sigma-Aldrich, USA), methanol (Merck, Germany), HPLC grade acetonitrile (MeCN, Sigma-Aldrich, USA), $NaBH_4$ (Merck, Germany), potassium tetrachloroplatinate(II) (K_2PtCl_4, Sigma-Aldrich, USA), perchloric acid ($HClO_4$, Sigma-Aldrich, USA), hydrazine hydrate (Merck, Germany). The ultra-pure water with resistance of 18.3 MU cm (Human Power 1+ Scholar purification system) was used in the experiments of aqueous media.

Instrumentation

All electrochemical experiments (CV and CA) were performed using IviumStat (USA) equipped with C3 cell stand. Electrochemical impedance spectroscopic experiments were carried out with a Gamry Reference 600 workstation equipped with a PCI4/300 potentiostat in conjunction with EIS 300 software. Modified electrodes were characterized in 1.0 mM ferrocyanide/1.0 mM ferricyanide ($[Fe(CN)_6]^{3-/4-}$) redox couple via EIS methods. EIS data were measured at 100 kHz to 0.1 Hz at 10 mV wave amplitude and at an electrode potential of 0.165 V, the formal potential of $[Fe(CN)_6]^{3-/4-}$ redox couple. Argon gas was passed through the solutions during experiments for about 10 min. JEOL 2100 transmission electron microscope (TEM) (JEOL Ltd., Tokyo, Japan) and ZEISS EVO 50 scanning electron microscope (SEM) (Germany) analytic microscopies were used to investigate the morphologies

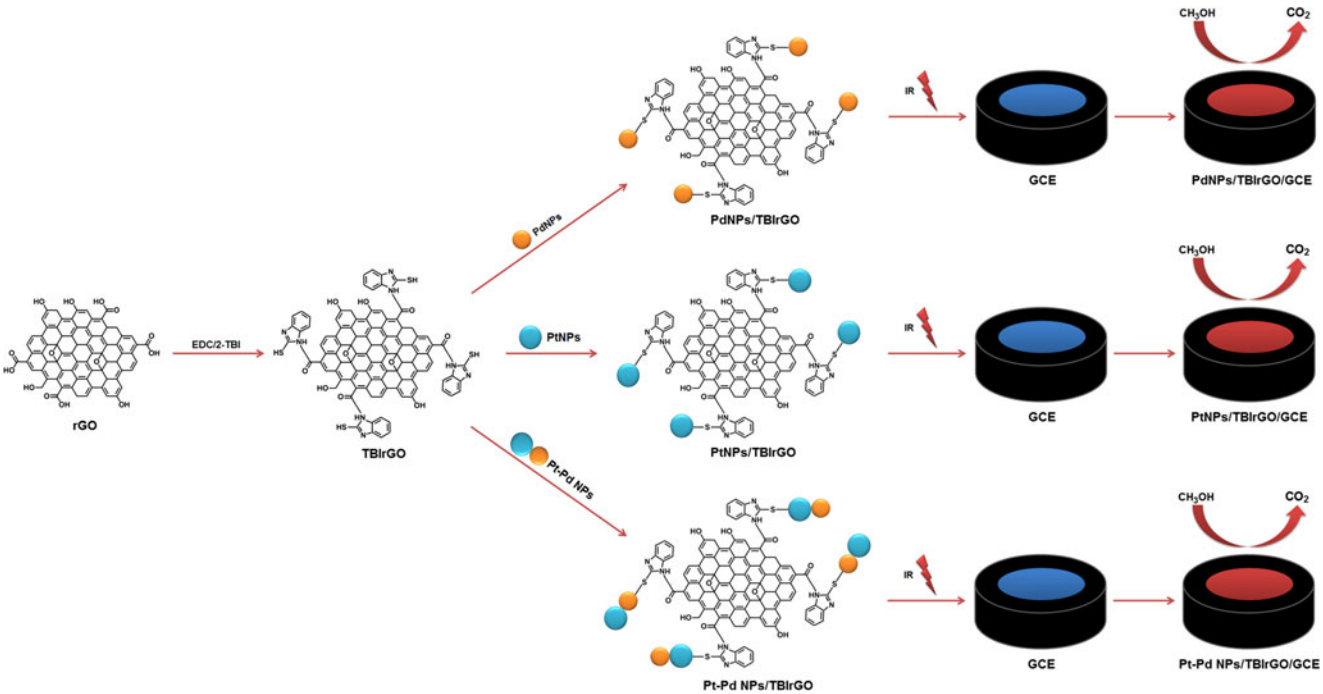

Scheme 1 The procedure of fabrication of the catalysts in present study

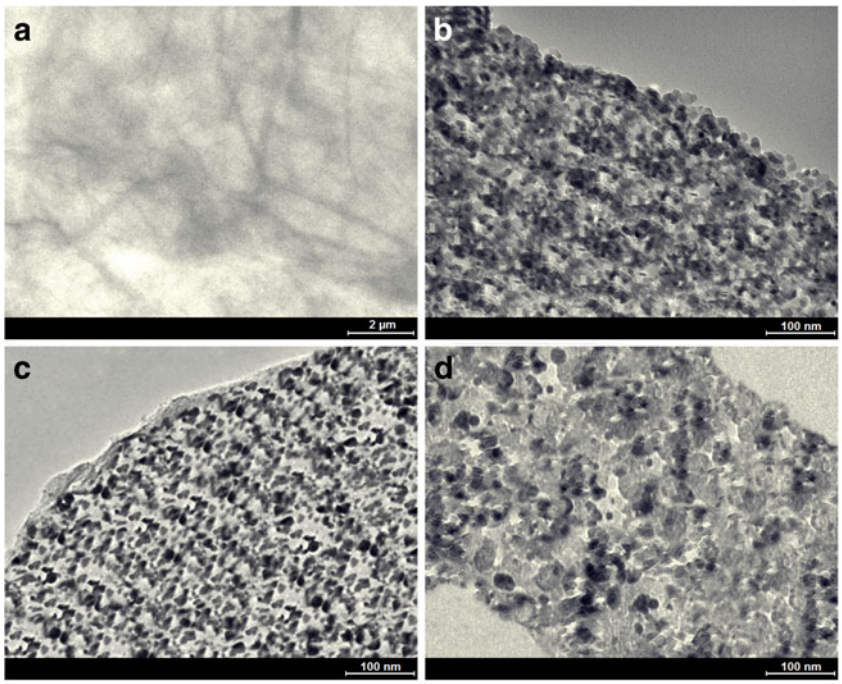

Fig. 1 TEM image of **a** rGO; **b** PtNPs/TBIrGO; **c** PdNPs/TBIrGO; **d** Pt-PdNPs/TBIrGO

of the nanocomposites. X-ray photo electron spectroscopy (XPS) analysis were performed on a PHI 5000 Versa Probe (F ULVAC-PHI, Inc., Japan/USA) model with monochromatized Al Ka radiation (1486.6 eV) as an X-ray anode operated at 50 W. To prepare the samples, one drop of the prepared nanocomposites was placed on clear glass and then dried in air. A Rigaku X-ray diffractometer was used for X-ray diffraction (XRD) measurements of the nanostructures.

Synthesis of rGO

Graphene oxide was synthesized according to our previous report [9]. The as-prepared GO was dispersed into 200 mL water. After that, hydrazine hydrate (80 wt%) of 4 mL was added and the solution was heated in an oil bath at 100 °C under a water-cooled condenser for 24 h. After the reaction, the prepared rGO product was collected by vacuum filtration. To carry out the surface activation of carboxylate groups of rGO, the rGO suspension was interacted with 0.2 M EDC solution for 8 h. Activated rGO suspension was mixed well with 1.0 mM TBI at a 1:1 volume ratio for 2 h (TBIrGO).

Synthesis of PdNPs, PtNPs, Pt-PdNPs, PtNPs/TBIrGO, PdNPs/TBIrGO and Pt-Pd NPs/TBIrGO

PdNPs were prepared by mixing 250 μL of 0.1 M Na_2PdCl_4 solution with 20 mg $NaBH_4$ solution [24]. PtNPs were prepared by mixing 200 μL of 0.1 M K_2PtCl_4 solution with 10 mg $NaBH_4$ solution. The solutions were kept in ultra-sonicated bath for 60 min [24]. To prepare bimetallic Pt-PdNPs, PtNPs and PdNPs solutions were mixed with volume ratio of 1:1. To prepare PtNPs/TBIrGO, PdNPs/TBIrGO and Pt-Pd NPs/TBIrGO nanocomposites, each of 1 mg mL^{-1} PtNPs, PdNPs and Pt-PdNPs solutions was dispersed homogenously in ultra-pure water mixed with 0.1 mg mL^{-1} of TBIrGO with volume ratio of 1:1. After that, the mixtures were kept in ultra-sonicated bath for 15 min. Finally, the

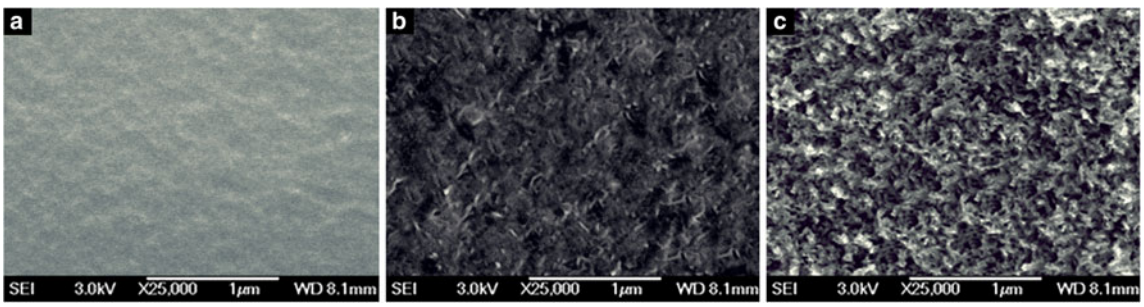

Fig. 2 SEM image of **a** bare GCE; **b** TBIrGO/GCE; **c** Pt-PdNPs/TBIrGO/GCE

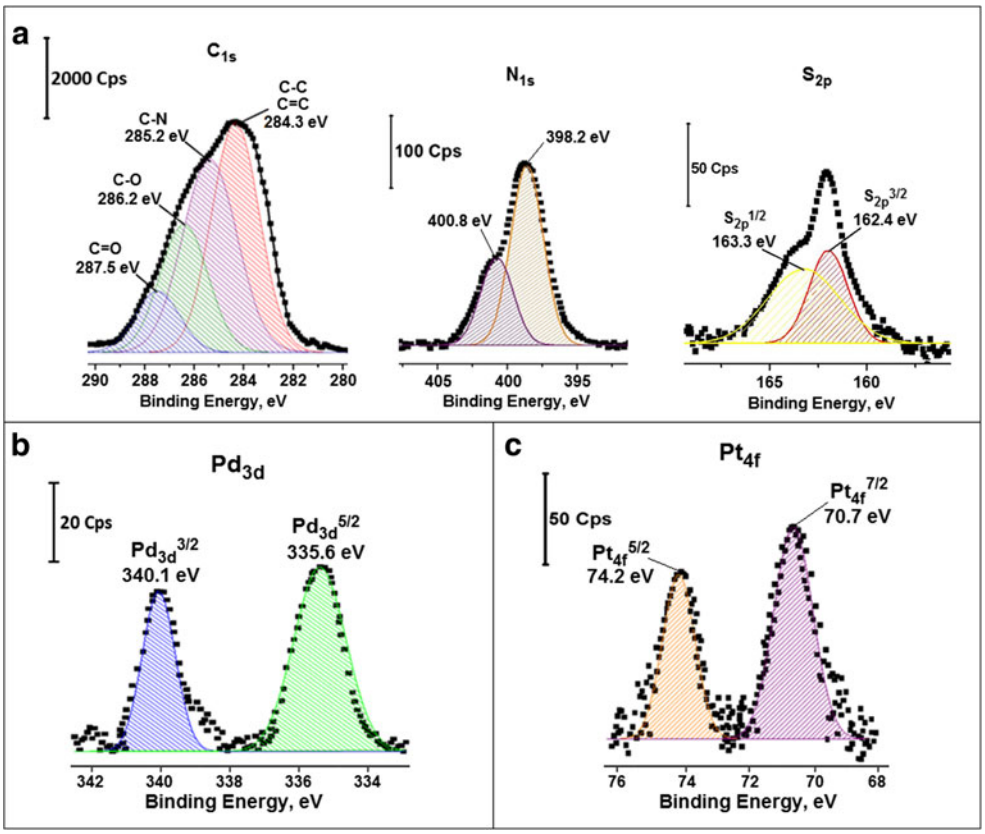

Fig. 3 The narrow region XPS spectra of **a** C_{1s}, N_{1s} and S_{2p} of TBIrGO; **b** Pd_{3d} of Pt-PdNPs/TBIrGO; **c** Pt_{4f} of Pt-PdNPs/TBIrGO

PtNPs/TBIrGO, PdNPs/TBIrGO and Pt-Pd NPs/TBIrGO nanocomposites were kept under room temperature.

Procedure for the electrode preparation

GCE was cleaned according to our previous reports [25, 26] and used as a working electrode. After that, the catalyst inks were prepared by dispersing 1 mg of catalyst (TBIrGO, PtNPs/TBIrGO, PdNPs/TBIrGO, Pt-PdNPs/TBIrGO) into 1 mL of ethanol via 20 min agitation. Fifteen microlitres of TBIrGO, PtNPs/TBIrGO, PdNPs/TBIrGO and Pt-PdNPs/TBIrGO suspensions was dropped onto the clean GCE surfaces. Then, the solvent was evaporated by an infrared lamp.

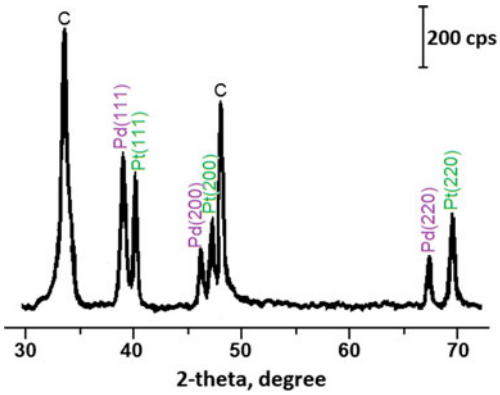

Fig. 4 XRD patterns of Pt-PdNPs/TBIrGO

The developed electrodes were stored in closed box without fluctuations of temperature and pressure. In addition, the voltammograms were obtained in an insulation cabinet for avoiding temperature and pressure fluctuation effect on the sensor response.

Electrochemical measurements

Electrocatalytic oxidation of 0.5 mol L^{-1} methanol on bare GCE, TBIrGO/GCE, PdNPs/TBIrGO/GCE, PtNPs/TBIrGO/GCE and Pt-PdNPs/TBIrGO/GCE was performed in

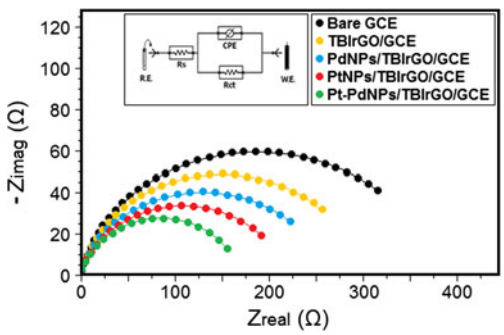

Fig. 5 Fitting of impedance spectrum for 1.0 mM $[Fe(CN)_6]^{3-/4-}$ (1:1) in 0.1 M KCl at bare GCE; TBIrGO/GCE; PdNPs/TBIrGO/GCE; PtNPs/TBIrGO/GCE; and Pt-PdNPs/TBIrGO/GCE: *inset* is the Randles equivalent circuit for Pt-PdNPs/TBIrGO/GCE. Frequency range is 100,000–0.1 Hz with 10 mV wave amplitude at a formal potential of 0.175 V. RE stands for reference electrode and WE for working electrode

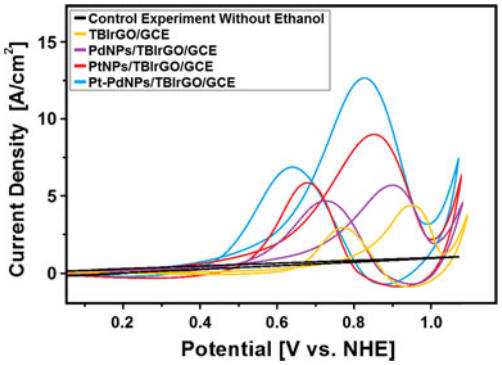

Fig. 6 Cyclic voltammograms of 0.5 mol L^{-1} methanol in 0.1 mol L^{-1} $HClO_4$ at TBIrGO/GCE; PdNPs/TBIrGO/GCE; PtNPs/TBIrGO/GCE and Pt-PdNPs/TBIrGO/GCE

0.1 mol L^{-1} $HClO_4$ by CV between −0.5 and +1.5 V. The Ag/AgCl and Pt wire electrodes were utilized as reference and counter electrode, respectively.

Results and discussion

Characterization of nanomaterial

The transparent and nano-sized rGO was shown in Fig. 1a–c showing the TEM images of the PtNPs/TBIrGO and PdNPs/TBIrGO nanocomposites which clearly demonstrate that dark PtNPs and PdNPs are well dispersed and attached on the sidewall of the TBIrGO. The average particle sizes of the PtNPs (Fig. 1b) and PdNPs (Fig. 1c) are very similar and the average lengths of the nanoparticles are 10–15 nm. The bimetallic Pt-PdNPs are shown in Fig. 1d. The excellent dispersion and anchoring of PtNPS and PdNPs are explained with the covalent functionalization of the carboxyl group of the rGO with TBI. That is corresponded to C–N groups in the covalent functionalization of the carboxyl group of the rGO with the amino group of the TBI (TBIrGO). The PtNPs with spherical PdNPs were distributed on lighter rGO sheets.

SEM characterization was performed for evaluations of the morphologies of the surfaces in step by step modification. The unmodified surface of GCE shown in Fig. 2a, b showed that the glassy carbon surface was covered with some slices. This situation indicated that glassy carbon surface was modified with TBI. The SEM graph of Pt-PdNPs/TBIrGO on GCE indicated that an intensive layer was observed (Fig. 2c). Hence, the successful binding of Pt-PdNPs was confirmed onto the surface.

Figure 3 shows the XPS spectrum of TBIrGO and Pt-PdNPs/TBIrGO nanocomposites. As seen in Fig. 3, C_{1s}, N_{1s}, S_{2p} peaks of TBIrGO (Fig. 3a), Pd_{3d} peaks of Pt-PdNPs/TBIrGO (Fig. 3b) and Pt_{4f} peaks of Pt-PdNPs/TBIrGO (Fig. 3c) confirmed that TBIrGO sheets were functionalized with Pt-PdNPs. As seen in Fig. 3a, the peaks at 284.3, 285.2 and 287.5 eV are related to C=C and C-N and C=O, respectively. The peak at 398.2 eV in the N_{1s} narrow region XPS spectrum corresponded to C-N groups in the covalent attachment of the carboxyl group of the rGO with the amino group of TBI. The peak at 400.8 eV corresponded to the N-H group in unreacted TBI molecules. The peak at 162.4 eV shows that the sulfur atom of the nanocomposite was grafted to the nanoparticles. The peak at 163.3 eV can be assigned to free mercapto group in unreacted TBI [3]. The signals of doublet $3d^{3/2}$ and $3d^{5/2}$ of Pd3d at 340.1 and 335.6 eV, respectively, indicated the presence of PdNPs on Pt-PdNPs/TBIrGO (Fig. 3b) [27]. The doublet $4f^{5/2}$ and $4f^{7/2}$ signals of Pt4f region appeared at 74.2 and 70.7 eV, respectively. These bands confirmed the presence of PtNPs on Pt-PdNPs/TBIrGO (Fig. 3c) [28].

The XRD pattern of Pt-PdNPs/TBIrGO nanocomposite is shown in Fig. 4. The intense and narrow peaks at $2\theta = 34.57°$ and 48.26° refers to the (002) and (004) planes of rGO sheets, respectively [29]. The characteristic peaks of PdNPs also have been observed. The three main peaks at $2\theta = 39.14°$, 46.17° and 67.58° corresponded to the (111), (200) and (220) planes of Pd, respectively [30]. The characteristic peaks of PtNPs also have been observed with the intense and narrow peak at $2\theta = 40.06°$ and the peaks at $2\theta = 47.52°$ and 69.83° corresponded to the (111), (200) and (220) planes of Pt, respectively [31].

Characterizations of modified glassy carbon electrodes by EIS

EIS is an effective method for probing the features of surface modified electrodes. It is capable of giving useful information about defects/holes existing on the modified surfaces, the kinetics and mechanism of the film formation processes and surface coverage [26, 32]. Figure 5 shows the impedance plot (Nyquist diagram) of bare GCE, TBIrGO/GCE, PdNPs/

Table 1 Comparison of methanol oxidation on modified electrodes in this study (scan rate, 50 mV s^{-1})

Electrode	If (A cm^{-2})	*E* (V)	Ib (A cm^{-2})	*E* (V)	If/Ib
Pt-PdNPs/TBIrGO/GCE	12.5 ± 0.07	0.83	7.35 ± 0.04	0.65	1.70
PtNPs/TBIrGO/GCE	9.0 ± 0.03	0.85	6.10 ± 0.04	0.68	1.48
PdNPs/TBIrGO/GCE	6.0 ± 0.02	0.90	4.4 ± 0.04	0.72	1.36
TBIrGO/GCE	4.3 ± 0.06	0.95	3.3 ± 0.02	0.78	1.30

TBIrGO/GCE, PtNPs/TBIrGO/GCE and Pt-PdNPs/TBIrGO/GCE. In addition, the inset of Fig. 5 shows the experimental data that are fitted to standard Randles equivalent circuits for Pt-PdNPs/TBIrGO/GCE surface analysis, which comprise the solution resistance (R_s), the charge transfer resistance (R_{ct}) and the constant phase element (CPE) for the cases of Pt-PdNPs/TBIrGO/GCE. The experimental impedance values are matched with Randles equivalent circuit simulation using Gamry software (EIS 300 Electrochemical Impedance Spectroscopy Software).

The EIS graph (Fig. 5) demonstrated that the value of charge transfer resistance (R_{ct}) of bare GCE was calculated as 375 Ω for $[Fe(CN)_6]^{3-/4-}$ redox couple solution. When the bare GCE was modified with TBIrGO, the value of R_{ct} was lower (300 Ω). Because of the lower value, we can say that the TBIrGO facilitated the rate of electron transfer between surface and solution. When TBIrGO nanocomposite was modified with PdNPs and PtNPs, the values of R_{ct} of PdNPs/TBIrGO/GCE and PtNPs/TBIrGO/GCE were lower than that of TBIrGO/GCE. According to the lower values of R_{ct}, PdNPs/TBIrGO and PtNPs/TBIrGO facilitated the rate of electron transfer in comparison to only TBIrGO film. The value of R_{ct} of Pt-PdNPs/TBIrGO/GCE was obtained as 170 Ω. Thus, the addition of bimetallic nanoparticles shows the more increase of catalytic activity, indicating the more active property of the Pt-PdNPs/TBIrGO film.

The effective surface areas (ESA) of different modified electrodes was obtained by CV with 1.0 mM $[Fe(CN)_6]^{3-}$ solution containing 0.1 M KCl as a probe at different scan rates according to the equation: $i_p = 2.69 \times 10^5\ A\ n^{3/2}\ D^{1/2}\ C\ v^{1/2}$, where i_p refers to the peak current and A is the electrode area (cm^2). For 1.0 mM $[Fe(CN)_6]^{3-}$, $n = 1$, $D = 7.6 \times 10^{-6}$ $cm^2\ s^{-1}$ (0.1 M KCl), C is the concentration of $[Fe(CN)_6]^{3-}$ and v is the scan rate. The ESA of TBIrGO/GCE, PdNPs/TBIrGO/GCE, PtNPs/TBIrGO/GCE and Pt-PdNPs/TBIrGO/GCE were calculated from the slope of the i_p versus $v^{1/2}$ plot to be 324, 578, 667 and 1189 cm^2/mg, respectively. These results show that the electrochemical surface area of the Pt-PdNPs/TBIrGO is 3.67, 2.06 and 1.78 times higher than those of TBIrGO, PdNPs/TBIrGO and PtNPs/TBIrGO, respectively. The high activity was explained by the small size of Pt-Pd NPs.

The electrocatalytic activities of the modified electrodes were also evaluated for 0.5 M methanol by CV in 0.1 mol L^{-1} $HClO_4$ at 50 mV s^{-1} (Fig. 6). In the case of the Pt-PdNPs/TBIrGO/GCE, a current peak of 12.5 ± 0.07 A cm^{-2} was observed during a forward anodic scan (If) at a potential of 0.83 V, while the reverse scan (Ib) showed a current peak of 7.35 ± 0.04 A cm^{-2} at 0.65 V. The efficiencies of the Pt-PdNPs/TBIrGO/GCE, PtNPs/TBIrGO/GCE, PdNPs/TBIrGO/GCE and TBIrGO/GCE on methanol oxidation were given in Table 1. The forward peak of Pt-PdNPs/TBIrGO/GCE was 1.39, 2.08 and 2.91 times higher

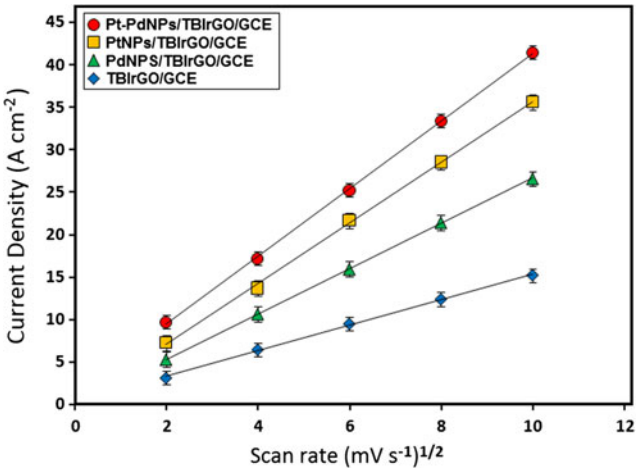

Fig. 7 The relationship of current density vs. the square root of scan rate at bare GCE; TBIrGO/GCE; PdNPs/TBIrGO/GCE; PtNPs/TBIrGO/GCE and Pt-PdNPs/TBIrGO/GCE

than those of PtNPs/TBIrGO/GCE, PdNPs/TBIrGO/GCE and TBIrGO/GCE, respectively. In addition, a control experiment of the Pt-PdNPs/TBIrGO/GCE in the electrolyte without methanol was completed (black curve of Fig. 6). According to the black curve, during the forward anodic scan and the reverse scan, no current peak was seen. Thus, the important activity enhancement in methanol oxidation is attributed to high active surface [33].

Figure 7 shows that the current density is proportional to the square root of the scan rate. This indicates that the electrochemical oxidation of methanol is diffusion processes at all surfaces. The slope for Pt-PdNPs/TBIrGO/GCE is larger than those for the other modified GCE. Thus, we can say that the diffusion process of methanol is fastest on the Pt-PdNPs/TBIrGO/GCE.

The chronoamperometry measurements were carried out to investigate the electrochemical performances of the prepared electrodes at 0.6 V in the presence of methanol. As shown in Fig. 8, all electrodes present current decay before steady current status is attained. The decay is possibly attributed to the fact that once the methanol oxidation reaction begins, some incomplete oxidation products adsorb on the catalyst surface

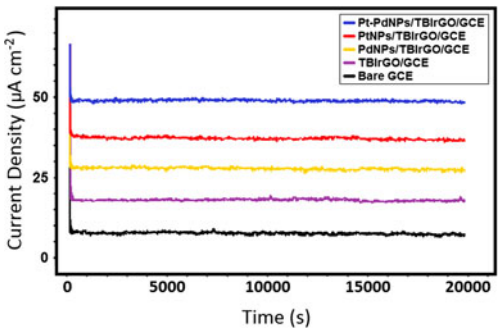

Fig. 8 Chronoamperometry results of 0.5 mol L^{-1} methanol in 0.1 mol L^{-1} $HClO_4$ at bare GCE; TBIrGO/GCE; PdNPs/TBIrGO/GCE; PtNPs/TBIrGO/GCE and Pt-PdNPs/TBIrGO/GCE at 0.6 V for 20,000 s

and poison it towards further methanol oxidation, which can also been observed in other studies [3, 22, 34, 35]. In the steady-state region, the current density of methanol oxidation on the Pt-PdNPs/TBIrGO/GCE is highest than that of methanol oxidation on the other electrodes. This indicates that the Pt-PdNPs/TBIrGO/GCE is a stable and poisoning-tolerance electrocatalyst for methanol oxidation.

The comparisons with the previous catalysts in the literature

The bimetallic Au-Pt alloyed nanochains supported on reduced graphene oxide (Au-Pt NCs/RGO) were prepared for DMFCs [36]. Three milligrams of the sample was dispersed into 1 mL of water and ultrasonicated for 30 min to obtain a homogeneous suspension. Then, 6 mL of the suspension was uniformly casted on the GCE surface. The ESA was calculated to be 32.43 m^2/g for Au-Pt NCs/RGO, which is not larger than that of Pt-PdNPs/TBIrGO (118.90 m^2/g).

Graphene oxide aerogel (GOA) was prepared to serve as catalyst support for Pt nanoparticles for methanol electrooxidation [37]. This catalyst (4.0 mg) had 95.50 m^2/g of ESA, which is not larger than that of Pt-PdNPs/TBIrGO (118.90 m^2/g).

Zhang et al. prepared Pd-Au-Ag nanoparticles supported on reduced graphene oxide (Pd-Au-Ag/RGO) [38]. The ESA value of the catalyst (4.0 mg) was 96.71 m^2/g, indicating more lower than of Pt-PdNPs/TBIrGO (118.90 m^2/g).

Ma et al. prepared rGO modified with 1,10-dimethyl-4,40-bipyridinium dichloride (methyl viologen, MV). After that, they performed immobilization of Pt nanoparticles to prepare a Pt/MV–RGO catalyst for direct methanol fuel cells [39]. The ESA values of Pt/MV–RGO (5 mg) and Pt/RGO (5 mg) were estimated to be 24.65 and 8.25 m^2/g, respectively, indicating more lower than Pt-PdNPs/TBIrGO (118.90 m^2/g).

Pt-SiO_2/graphene nanocomposites (Pt-SiO_2-G) have been synthesized under solvothermal conditions [40]. The ESA value and If/Ib value of Pt-SiO_2-G (5 mg) were estimated to be 87.19 m^2/g and 1.04, respectively, indicating that the best catalyst in this study shows more electrocatalytic activity towards methanol oxidation.

Conclusions

A new and cost-effective catalysts based on bimetallic nanoparticle using a minimal amount of the precious metal was developed for the production of a working electrode that can be utilized in DMFCs. The catalysts were successfully prepared and modified on GCE surfaces in the present study. According to the results of EIS and CV, the prepared nanocomposites based on bimetallic nanoparticles showed catalytic activity towards methanol as the fuel. Especially, the Pt-PdNPs/TBIrGO catalyst provides an opportunity to prepare a promising electrode with a large active surface area of 118.90 m^2/g, high electro-oxidative activity and superior CO tolerance than the PtNPs/TBIrGO, PDNPs/TBIrGO and TBIrGO catalysts. In addition, the performance of the Pt-PdNPs/TBIrGO catalyst is higher than those of catalysts in the mentioned literatures such as current densities on forward anodic scan and the reverse scan, the ratio of the forward and backward anodic peak current densities.

References

1. Gupta VK, Yola ML, Atar N, Üstündağ Z, Solak AO (2014) Electrochemical studies on graphene oxide-supported metallic and bimetallic nanoparticles for fuel cell applications. J Mol Liq 191: 172–176. doi:10.1016/j.molliq.2013.12.014
2. Ahn K, Kim M, Kim K, Ju H, Oh I, Kim J (2015) Fabrication of low-methanol-permeability sulfonated poly(phenylene oxide) membranes with hollow glass microspheres for direct methanol fuel cells. J Power Sources 276:309–319. doi:10.1016/j.jpowsour.2014.11.114
3. Atar N, Eren T, Yola ML, Karimi-Maleh H, Demirdogen B (2015) Magnetic iron oxide and iron oxide@gold nanoparticle anchored nitrogen and sulfur-functionalized reduced graphene oxide electrocatalyst for methanol oxidation. RSC Advances 5(33): 26402–26409. doi:10.1039/C5RA03735B
4. Rashid M, Jun T-S, Jung Y, Kim YS (2015) Bimetallic core–shell Ag@Pt nanoparticle-decorated MWNT electrodes for amperometric H2 sensors and direct methanol fuel cells. Sensors Actuators B Chem 208:7–13. doi:10.1016/j.snb.2014.11.005
5. Yola ML, Eren T, Atar N, Wang S (2014) Adsorptive and photocatalytic removal of reactive dyes by silver nanoparticle-colemanite ore waste. Chem Eng J 242:333–340. doi:10.1016/j.cej.2013.12.086
6. Yola ML, Atar N (2014) A novel voltammetric sensor based on gold nanoparticles involved in p-aminothiophenol functionalized multi-walled carbon nanotubes: application to the simultaneous determination of quercetin and rutin. Electrochim Acta 119:24–31. doi:10.1016/j.electacta.2013.12.028
7. Gupta VK, Yola ML, Eren T, Kartal F, Çağlayan MO, Atar N (2014) Catalytic activity of Fe@Ag nanoparticle involved calcium alginate beads for the reduction of nitrophenols. J Mol Liq 190: 133–138. doi:10.1016/j.molliq.2013.10.022
8. Yola ML, Eren T, Atar N (2014) A novel efficient photocatalyst based on TiO_2 nanoparticles involved boron enrichment waste for photocatalytic degradation of atrazine. Chem Eng J 250:288–294. doi:10.1016/j.cej.2014.03.116
9. Yola ML, Eren T, Atar N (2015) A sensitive molecular imprinted electrochemical sensor based on gold nanoparticles decorated graphene oxide: application to selective determination of tyrosine in milk. Sensors Actuators B Chem 210:149–157. doi:10.1016/j.snb.2014.12.098
10. Sanghavi B, Wolfbeis O, Hirsch T, Swami N (2015) Nanomaterial-based electrochemical sensing of neurological drugs and neurotransmitters. Microchim Acta 182(1–2):1–41. doi:10.1007/s00604-014-1308-4
11. Sanghavi BJ, Srivastava AK (2010) Simultaneous voltammetric determination of acetaminophen, aspirin and caffeine using an in situ surfactant-modified multiwalled carbon nanotube paste

electrode. Electrochim Acta 55(28):8638–8648. doi:10.1016/j.electacta.2010.07.093
12. Sanghavi BJ, Mobin SM, Mathur P, Lahiri GK, Srivastava AK (2013) Biomimetic sensor for certain catecholamines employing copper(II) complex and silver nanoparticle modified glassy carbon paste electrode. Biosens Bioelectron 39(1):124–132. doi:10.1016/j.bios.2012.07.008
13. Sanghavi BJ, Varhue W, Chávez JL, Chou C-F, Swami NS (2014) Electrokinetic preconcentration and detection of neuropeptides at patterned graphene-modified electrodes in a nanochannel. Anal Chem 86(9):4120–4125. doi:10.1021/ac500155g
14. Sanghavi BJ, Sitaula S, Griep MH, Karna SP, Ali MF, Swami NS (2013) Real-time electrochemical monitoring of adenosine triphosphate in the picomolar to micromolar range using graphene-modified electrodes. Anal Chem 85(17):8158–8165. doi:10.1021/ac4011205
15. Kim S, Sohn H-J, Park S-J (2010) Preparation and characterization of carbon-related materials supports for catalysts of direct methanol fuel cells. Curr Appl Phys 10(4):1142–1147. doi:10.1016/j.cap.2010.01.016
16. Yola ML, Eren T, Atar N (2014) A novel and sensitive electrochemical DNA biosensor based on Fe@Au nanoparticles decorated graphene oxide. Electrochim Acta 125:38–47. doi:10.1016/j.electacta.2014.01.074
17. Yola ML, Gupta VK, Eren T, Şen AE, Atar N (2014) A novel electro analytical nanosensor based on graphene oxide/silver nanoparticles for simultaneous determination of quercetin and morin. Electrochim Acta 120:204–211. doi:10.1016/j.electacta.2013.12.086
18. Yola ML, Eren T, Atar N (2014) Molecularly imprinted electrochemical biosensor based on Fe@Au nanoparticles involved in 2-aminoethanethiol functionalized multi-walled carbon nanotubes for sensitive determination of cefexime in human plasma. Biosens Bioelectron 60:277–285. doi:10.1016/j.bios.2014.04.045
19. Gupta VK, Atar N, Yola ML, Üstündağ Z, Uzun L (2014) A novel magnetic Fe@Au core–shell nanoparticles anchored graphene oxide recyclable nanocatalyst for the reduction of nitrophenol compounds. Water Res 48:210–217. doi:10.1016/j.watres.2013.09.027
20. Eren T, Atar N, Yola ML, Karimi-Maleh H, Çolak AT, Olgun A (2015) Facile and green fabrication of silver nanoparticles on a polyoxometalate for Li-ion battery. Ionics 21(8):2193–2199. doi:10.1007/s11581-015-1409-z
21. Sanghavi BJ, Hirsch G, Karna SP, Srivastava AK (2012) Potentiometric stripping analysis of methyl and ethyl parathion employing carbon nanoparticles and halloysite nanoclay modified carbon paste electrode. Anal Chim Acta 735:37–45. doi:10.1016/j.aca.2012.05.029
22. Gu CD, Huang ML, Ge X, Zheng H, Wang XL, Tu JP (2014) NiO electrode for methanol electro-oxidation: mesoporous vs. nanoparticulate. Int J Hydrog Energy 39(21):10892–10901. doi:10.1016/j.ijhydene.2014.05.028
23. Atar N, Eren T, Yola ML, Gerengi H, Wang S (2015) Fe@Ag nanoparticles decorated reduced graphene oxide as ultrahigh capacity anode material for lithium-ion battery. Ionics. doi:10.1007/s11581-015-1520-1
24. Yang G, Zhou Y, Pan H-B, Zhu C, Fu S, Wai CM, Du D, Zhu J-J, Lin Y (2016) Ultrasonic-assisted synthesis of Pd–Pt/carbon nanotubes nanocomposites for enhanced electro-oxidation of ethanol and methanol in alkaline medium. Ultrason Sonochem 28:192–198. doi:10.1016/j.ultsonch.2015.07.021
25. Gupta VK, Yola ML, Özaltın N, Atar N, Üstündağ Z, Uzun L (2013) Molecular imprinted polypyrrole modified glassy carbon electrode for the determination of tobramycin. Electrochim Acta 112:37–43. doi:10.1016/j.electacta.2013.08.132
26. Yola ML, Atar N, Qureshi MS, Üstündağ Z, Solak AO (2012) Electrochemically grafted etodolac film on glassy carbon for Pb(II) determination. Sensors Actuators B Chem 171–172:1207–1215. doi:10.1016/j.snb.2012.06.082
27. Wojcieszak R, Genet MJ, Eloy P, Ruiz P, Gaigneaux EM (2010) Determination of the size of supported Pd nanoparticles by X-ray photoelectron spectroscopy. Comparison with X-ray diffraction, transmission electron microscopy, and H2 chemisorption methods. J Phys Chem C 114(39):16677–16684. doi:10.1021/jp106956w
28. Dablemont C, Lang P, Mangeney C, Piquemal J-Y, Petkov V, Herbst F, Viau G (2008) FTIR and XPS study of Pt nanoparticle functionalization and interaction with alumina. Langmuir 24(11):5832–5841. doi:10.1021/la7028643
29. Bradder P, Ling SK, Wang S, Liu S (2011) Dye adsorption on layered graphite oxide. J Chem Eng Data 56(1):138–141. doi:10.1021/je101049g
30. Liu Y, Liu L, Shan J, Zhang J (2015) Electrodeposition of palladium and reduced graphene oxide nanocomposites on foam-nickel electrode for electrocatalytic hydrodechlorination of 4-chlorophenol. J Hazard Mater 290:1–8. doi:10.1016/j.jhazmat.2015.02.016
31. Yang B, Bin D, Wang H, Zhu M, Yang P, Du Y (2015) High quality Pt-graphene nanocomposites for efficient electrocatalytic nitrite sensing. Colloids Surf A Physicochem Eng Asp 481:43–50. doi:10.1016/j.colsurfa.2015.04.027
32. Gupta VK, Yola ML, Atar N, Solak AO, Uzun L, Üstündağ Z (2013) Electrochemically modified sulfisoxazole nanofilm on glassy carbon for determination of cadmium(II) in water samples. Electrochim Acta 105:149–156. doi:10.1016/j.electacta.2013.04.136
33. Su L, Jia W, Li C-M, Lei Y (2014) Mechanisms for enhanced performance of platinum-based electrocatalysts in proton exchange membrane fuel cells. ChemSusChem 7(2):361–378. doi:10.1002/cssc.201300823
34. Tong YY, Gu CD, Zhang JL, Huang ML, Tang H, Wang XL, Tu JP (2015) Three-dimensional astrocyte-network Ni-P-O compound with superior electrocatalytic activity and stability for methanol oxidation in alkaline environments. J Mater Chem A 3(8):4669–4678. doi:10.1039/C4TA06697A
35. Atar N, Eren T, Demirdögen B, Yola ML, Çağlayan MO (2015) Silver, gold, and silver@gold nanoparticle-anchored l-cysteine-functionalized reduced graphene oxide as electrocatalyst for methanol oxidation. Ionics 21(8):2285–2293. doi:10.1007/s11581-015-1395-1
36. Chen D-J, Zhang Q-L, Feng J-X, Ju K-J, Wang A-J, Wei J, Feng J-J (2015) One-pot wet-chemical co-reduction synthesis of bimetallic gold–platinum nanochains supported on reduced graphene oxide with enhanced electrocatalytic activity. J Power Sources 287:363–369. doi:10.1016/j.jpowsour.2015.04.080
37. Duan J, Zhang X, Yuan W, Chen H, Jiang S, Liu X, Zhang Y, Chang L, Sun Z, Du J (2015) Graphene oxide aerogel-supported Pt electrocatalysts for methanol oxidation. J Power Sources 285:76–79. doi:10.1016/j.jpowsour.2015.03.064
38. Zhang L, Wang H, Li X, Xia F, Liu Y, Xu X, Gao J, Xing F (2015) One-step synthesis of palladium-gold-silver ternary nanoparticles supported on reduced graphene oxide for the electrooxidation of methanol and ethanol. Electrochim Acta 172:42–51. doi:10.1016/j.electacta.2014.11.152
39. Ma J, Wang L, Mu X, Cao Y (2015) Enhanced electrocatalytic activity of Pt nanoparticles supported on functionalized graphene for methanol oxidation and oxygen reduction. J Colloid Interface Sci 457:102–107. doi:10.1016/j.jcis.2015.06.031
40. Vu THT, Tran TTT, Le HNT, Tran LT, Nguyen PHT, Nguyen HT, Bui NQ (2015) Solvothermal synthesis of Pt -SiO2/graphene nanocomposites as efficient electrocatalyst for methanol oxidation. Electrochim Acta 161:335–342. doi:10.1016/j.electacta.2015.02.100